Article

Long-Term Comparison of Two- and Three-Dimensional Computed Tomography Analyses of Cranial Bone Defects in Severe Parietal Thinning

Johannes Dominikus Pallua[1*], Anton Kasper Pallua[2], Werner Streif[3], Harald Spiegl[4], Clemens Halder[4], Rohit Arora[1] and Michael Schirmer[5*]

[1] University Hospital for Orthopaedics and Traumatology, Medical University of Innsbruck, Anichstraße 35, 6020 Innsbruck, Austria; rohit.arora@tirol-kliniken.at; johannes.pallua@i-med.ac.at
[2] Former Institute for Computed Tomography-Neuro CT, Medical University of Innsbruck, Anichstraße 35, 6020 Innsbruck, Austria; anton.k.pallua@cnh.at
[3] Department of Pediatrics I, Medical University of Innsbruck, Anichstrasse 35, 6020 Innsbruck, Austria; werner.streif@i-med.ac.at
[4] WESTCAM Datentechnik GmbH, Gewerbepark 38, 6068 Mils, Austria; harald.spiegl@westcam.at; clemens.halder@westcam.at
[5] Department of Internal Medicine, Clinic II, Medical University of Innsbruck, Anichstrasse 35, 6020 Innsbruck, Austria; michael.schirmer@i-med.ac.at
* Correspondence: johannes.pallua@i-med.ac.at; schirmer.michael@icloud.com

Abstract: Quantification of bone loss for follow-up comparisons has not been routinely performed in patients with parietal thinning so far. This study compares different methodological approaches including both 2- and 3-dimensional methods in computerized tomographies of a single patient. The 2-dimensional method provides accurate measurements of bone thickness, while the 3-dimensional method allows for a more comprehensive view of the bone's structure, including parameters like shape, size, and thickness. The techniques provided valuable data for the treating physician and suggest a possible effect of corticosteroids in this individual patient. The study concludes that 3-dimensional reconstruction of computerized tomographies with subsequent 2-dimensional analyses appears justified for routine radiological practice to increase clinical awareness of the size of the parietal bone defects and allow for quantification of bone loss during long-term follow-ups. Further validation of the proposed analytical approaches is warranted in larger studies to investigate patterns of bone thinning across the skull and changes in bone volumes over time, with specialized software to be approved for such analyses.

Keywords: parietal thinning; measurement reliability; bone defects; magnetic resonance imaging; computer tomography; osteology; rheumatology; rare disease

1. Introduction

The human parietal bone is essential in the skull, forming part of the skullcap. Biparietal thinning, also known as biparietal osteodystrophy, is characterized by extreme bone thinning in the parietal bones, located between the sagittal suture and the parietal prominence and anteriorly to the parietal foramina [1,2]. Sometimes, a "sulcus" is observed along the sagittal suture. This condition is usually expressed symmetrically and bilaterally and can be classified into a simple flat type and a groove or crater-like type [1,2]. The prevalence of biparietal thinning is between 0.25% and 0.8% [1,3]. Biparietal thinning is common in older (postmenopausal) females, although it may also occur in males and children [1,4,5]. This aspect differs from Paget's disease, which shows a male: female ratio of 3:2 when using sex-standardized prevalence rates [6]. Although first described in 1783, the etiology of biparietal thinning remains unknown [1]. Parietal skull thinning is a complex phenomenon involving bone density, structure, and composition changes. Various theories have been proposed by anatomists, pathologists, anthropologists, physicians, and radiologists. Several factors have been proposed as relevant to its development. These include age-related bone loss, hormonal changes, genetic predisposition, and nutritional deficiencies. In addition, certain medical conditions such as

 doi:10.20944/preprints202304.0749.v1

osteoporosis, Paget's disease, and hyperparathyroidism have also been associated with parietal skull thinning and syphilis, tumors, external pressure, muscular stimuli, and the friction of the galea aponeurotica [2,7-9]. Tumors, for example, can cause bone loss through direct invasion or indirectly by releasing cytokines that stimulate bone resorption. Some cases of parietal thinning have been observed with suspected genetic backgrounds in families, but the role of genetics has not been established so far [4,10].

In summary, biparietal thinning is a pathological lesion characterized by extreme bone thinning in the parietal bones. Decreased bone density and quality can increase the risk of skull fractures. For diagnostic purposes, radiographic imaging has been used to evaluate biparietal thinning, including conventional X-ray, computed tomography (CT), magnetic resonance imaging (MRI), and bone scintigraphy [3,4,11,12]. These techniques can provide detailed structural information about the thickness and density of the parietal bone with CT and MRI and signs of metabolic activity when using bone scintigraphy. Conventional radiography is the most widely used imaging modality for evaluating bone loss as it is inexpensive, readily available, and with good visualization of bony structures. However, conventional radiography has limited sensitivity for the early detection of bone loss and cannot provide quantitative data on bone density. More sensitive imaging modalities to detect bone loss are CT and MRI. While CT is ideal for evaluating the extent and severity of bone loss, it exposes the patient to ionizing radiation and is more expensive than conventional radiography. MRI, however, does not expose the patient to ionizing radiation and is better suited for evaluating soft tissues and bone marrow, but it has limited spatial resolution and may not provide sufficient details for assessing bone density [13]. Quantitative measures of bone density, such as bone mineral density (BMD) using dual-energy X-ray absorptiometry (DXA) or other specialized techniques, are certainly not sensitive enough for the skull. DXA is a specialized imaging modality measuring BMD, especially at the radius, the hips, and the spine. It is the gold standard for diagnosing osteoporosis and is recommended by the World Health Organization for routine screening in postmenopausal women and men over 50 [14]. Combined, diagnosis of parietal skull thinning typically requires imaging studies with quantitative measures of bone density. The choice of imaging modalities depends on the clinical question, availability of resources, and patient factors, and a multi-modality approach may be preferred for some cases. The present investigation aims to further analyze images with quantification of chronic parietal skull thinning over two years. This report compares the descriptive approach to CT images with 2-dimensional (2D) and 3-dimensional (3D) techniques before and after corticosteroid treatment. In patients with parietal thinning, improved analyses of CT images may provide essential information for the treating physicians.

2. Materials and Methods

2.1. Patient's assessment and follow-up with multimodal diagnostics

A 72-year-old female patient presented at the rheumatology outpatient clinic with recurrent headaches. Headaches occurred together with the development of subjective bony swellings on the skull. History revealed subtotal gastrectomy with T1 lymph node dissection because of a malignant neoplasm (stage pT1(a)N0M0; R0; G3; L0; V0, UICC Ia) three years earlier, which still was in ongoing remission after the clinical screening with additional gastroscopy, the first CT and another ^{18}F-Fluorodexoyglucose positron emission tomography (FDG-PET)-CT during follow-up.

As the patient had noticed parietal changes for 1 year, ^{99m}Technetium scintigraphy, MRI, and CT imaging were performed. The MR confirmed not only the irregularities of the skull but also showed chronic vascular leucencephalopathic changes. Endocrinology had diagnosed hyperparathyroidism (with an elevated level of 88.1 ng/L for parathormone with upper normal level of 65 ng/L), and ruled out typical osteodystrophy deformans (Paget's disease) based on the ^{99m}Technetium scintigraphy and MRI. Osteoporosis was diagnosed in the lumbar spine with a T score of -2.6, and osteopenia of the femur (T = -1.8) using DXA (HOLOGIC), but without the need for bone-specific treatment as argued according to the current guideline of the "Dachverband Osteologie" [15]. A dermatologic visit with histology of a capillitium skin biopsy (including dermis and minimal subcutis) had shown cicatrized

 doi:10.20944/preprints202304.0749.v1

inflammatory reactions around the hair follicles with diffuse lymhocytic infiltrates, scarring alopecia and Lichen ruber, type planopilaris, which was not suspected as the underlying cause of parietal thinning. A neurological visit ruled out any neurological disease as the underlying cause of parietal thinning. From the clinical perspective, the patient was otherwise healthy, especially without any elevated markers for inflammation (erythrocyte sedimentation rate and C-reactive protein) in the serum or any vascular risk factors, including arterial hypertension, diabetes mellitus, obesity or smoking history.

Considering the diffuse lymphocytic infiltrates as possible triggers of parietal thinning, the patient was informed about the potential benefits and risks of immunosuppression, specific corticosteroids as a rapidly acting immune-suppressive agent. After shared decision-making, 40mg of methylprednisolone was rapidly tapered to 8mg, with a marked reduction of headaches both in the frequency of occurrence and severity. Besides, biphosphonates were recommended for the treatment of osteoporosis. CT was repeated at days 185, 229, and 275 to assess further bone loss as side-effect of corticosteroids to assess possible worsening of parietal thinning.

2.2. Computed tomography imaging

CT images were obtained with a CT scanner (SIEMENS SOMATOM Confidence; Siemens, Erlangen, Germany). The patient head was scanned with a tube voltage of 120 kVp, a maximum X-ray tube current of 184 mA, an X-ray tube current of 112 mA, an exposure time per rotation of 1 s, a nominal single collimation width of 0.6 mm, a nominal total collimation width of 12 mm and a pitch factor of 0.55.

2.3. *Application of quantification methods for image analyses*

Image analyses were performed using CT data sets from 4 different time points. The reconstructions were carried out using Analyze 14.0 (Biomedical Imaging Resources, Mayo Foundation, Rochester, NY, USA) and GOM Inspect (GOM Inspect® v8, GOM GmbH, Braunschweig, Germany) software. In the first stage of the assessment, the head CT scans were reconstructed by semi-automatic object segmentation with region grow (minimum 319, maximal 3071).

2.3.1. Two-dimensional (2D) measurement methods

2D measurements were based on analyzing the CT data gained with multiplanar reconstructions. The image was set in three planes: frontal, sagittal, and transverse, and measurements were performed with the sample point tool and the sample line tool. The sample line tool defines a line on a 2D image or a 3D rendering. The tool reports distance measurements, line intensity profile, and the coordinates of the line endpoints. The sample point tool allows to selection of points on the 2D image data or 3D rendering (Figure 1). The tool reports the coordinates and intensity value of the selected point.

Preprints (www.preprints.org) | NOT PEER-REVIEWED | Posted: 23 April 2023 doi:10.20944/preprints202304.0749.v1

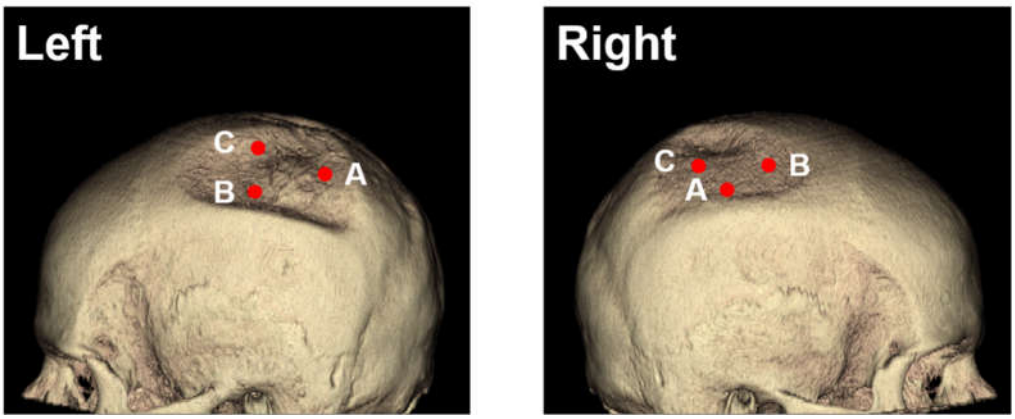

Figure 1. Selection of sample points on the left and right side for 2D measurements in 3D head models using CT images in the lateral views.

2.3.2. Computed tomography osteoabsorptiometry (CT-OAM)

Computed tomography osteoabsorptiometry (CT-OAM) is a non-invasive technique that can reveal information about the density distribution. In contrast to conventional methods of CT densitometry, which measure absolute values for bone density in large areas, CT-OAM can demonstrate the relative distribution over the entire surface using a false-colour diagram. This technique allows for detecting differences in relative distribution [16-19]. CT-OAM was evaluated using Analyze 14.0 (Biomedical Imaging Resources, Mayo Foundation, Rochester, NY, USA). Skulls CT datasets were registered with 2-D transformation using linear interpolation and manually segmented before the data were false colour-coded and superimposed on the 3-dimensionally reconstructed for anatomical localization of the mineral bone density creating a bone mineral density densitogram. The maximum intensity projection revealed the HU of each pixel to a depth of 190 slices (149.570 mm), and threshold values was chosen to be ≤ 300 to ≥ 1300 HU.

2.3.3. Analysis of densitogram patterns

Analysis of densitogram patterns was adapted from Poilliot A. et al. and Gay M.H. et al. [16,20]. The skull's mineral density pattern over time was evaluated based on the mean HU values of the regions on the densitogram for each dataset. The skull surface was subdivided into three regions: Os parietal left and right and sutura sagittalis. Zones with low mineralization were defined as those with 301 to 400 HU. These lower mineralization zones were identified by generating a black-white image with a threshold cut-off at 500 HU using Fiji [21]. The regions with low HU values were identified based on their anatomical location with automatic particle counting using Fiji.

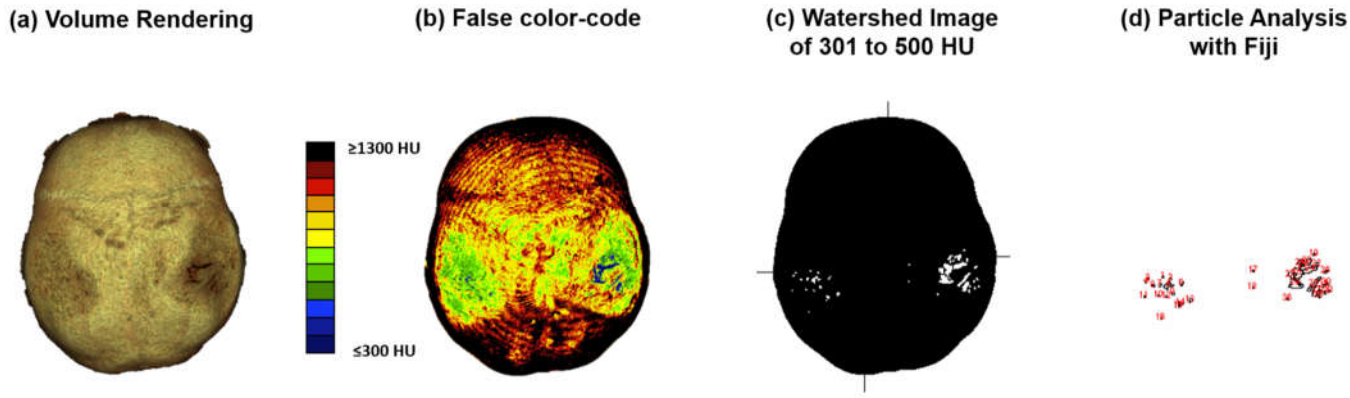

Figure 2. CT-OAM methodology. (**a**) CT data were uploaded to the image analysis software ANALYZE® 14.0. The skulls were registered with 2-D transformation using linear interpolation and reconstructed three-dimensionally. (**b**) Greyscale values corresponding to the respective HU were

Preprints (www.preprints.org) | NOT PEER-REVIEWED | Posted: 23 April 2023 doi:10.20944/preprints202304.0749.v1

surface-projected using a Maximum Intensity Projection (MIP) algorithm generating a greyscale densitogram. A false color code corresponding to the HU units was applied. (**c**) to (**d**) The MIP color-code images were loaded into Fiji. The Images were color split, threshold adapted, watershed separated, and particles with 301 to 500 HU analyzed.

2.3.4. Three-dimensional (3D) measurement method

For 3D measurements based on CT data, all scans were reconstructed in three-dimensional space using the 3D Slicer software (3D Slicer ver 4.4). The program allowed the conversion of a DICOM file into a Mesh file, which could be further evaluated using the GOM Inspect (GOM Inspect® v8, GOM GmbH, Braunschweig, Germany) software. One observer conducted 3D reconstruction to avoid any errors associated with the 3D reconstruction itself. The CT scans were marked as "model" and converted into the computer-aided design (CAD) format, while the second tomogram, called "comparative," was converted into the Mesh format, a universal file format for geometry. Both models were compared using the GOM Inspect (GOM GmbH, Braunschweig, Germany) program (Figure 2). Next, all reconstructed skulls were aligned over the red-marked area. The parietal bone thickness itself was then measured in the three defined positions for every time point. Finally, the volumes of bone loss were calculated for both sides.

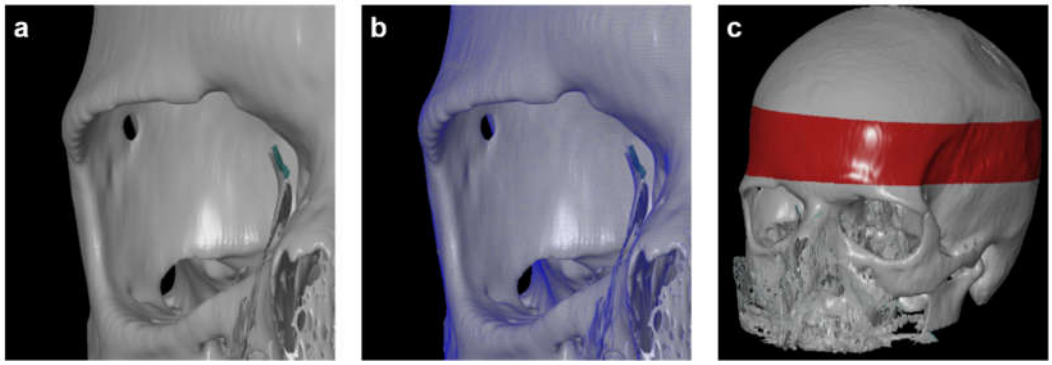

Figure 2. (**a**) Computer-aided design (CAD) model. (**b**) Overlay of CAD model with Mesh format. (**c**) skull alignment. The 3D reconstruction is reliable, with average differences between the two models not exceeding 0.15 mm.

2.4. Statistical analyses

This study was guided by an earlier study on the reliability of glenoid bone defect measurements on 2D and 3D CT [22]. Accordingly, two models were applied to test intra- and inter-observer reliability. Besides, we added an observer (an orthopedic surgeon) to present the reliability of measurements performed by observers with the same level of expertise. Thus three independent researchers at different levels of experience were involved.

Statistical analysis was performed using GraphPad Prism (version 9, San Diego, CA, USA) and SPSS software (IBM ver. 22.0.0.1). After testing for normal distribution, linear and volumetric measurements were compared over time using the one way ANOVA test using the Fisher's LSD test with p-values < 0.05 considered as significant.

Preprints (www.preprints.org) | NOT PEER-REVIEWED | Posted: 23 April 2023 doi:10.20944/preprints202304.0749.v1

3. Results

3.1. Descriptive imaging reports before and after 3D - reconstruction

Without reconstruction, the skull of the first CT was described as asymmetric parietal thinning of the left side as a normal variant. Retrospective 3D - reconstruction of the CT revealed further details of the normal variant, with impressive defects at both sites of the skull (Figures 1 and 3). These findings were confirmed in the subsequent CTs performed on days 185, 229, and 275.

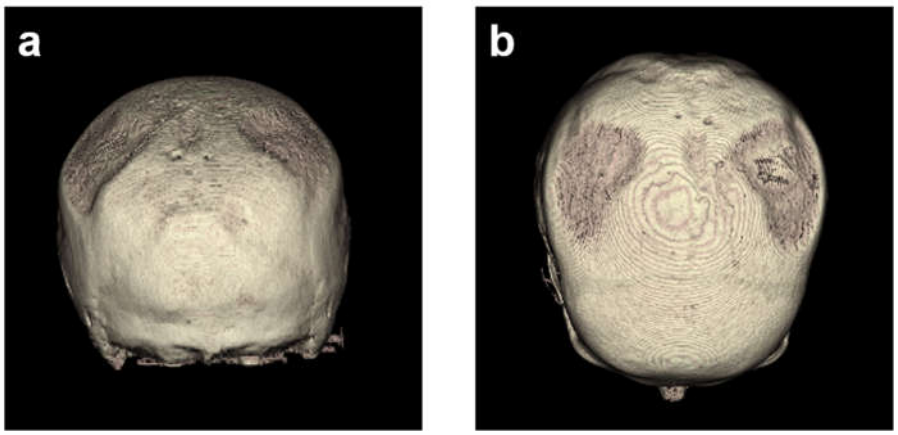

Figure 3. 3D head models based on first CT images with reconstruction by semi-automatic object segmentation with region grow in a caudal (**a**) and dorsal view (**b**) displaying the parietal cranial bone. The corresponding lateral left and lateral right views are shown in Figure 1.

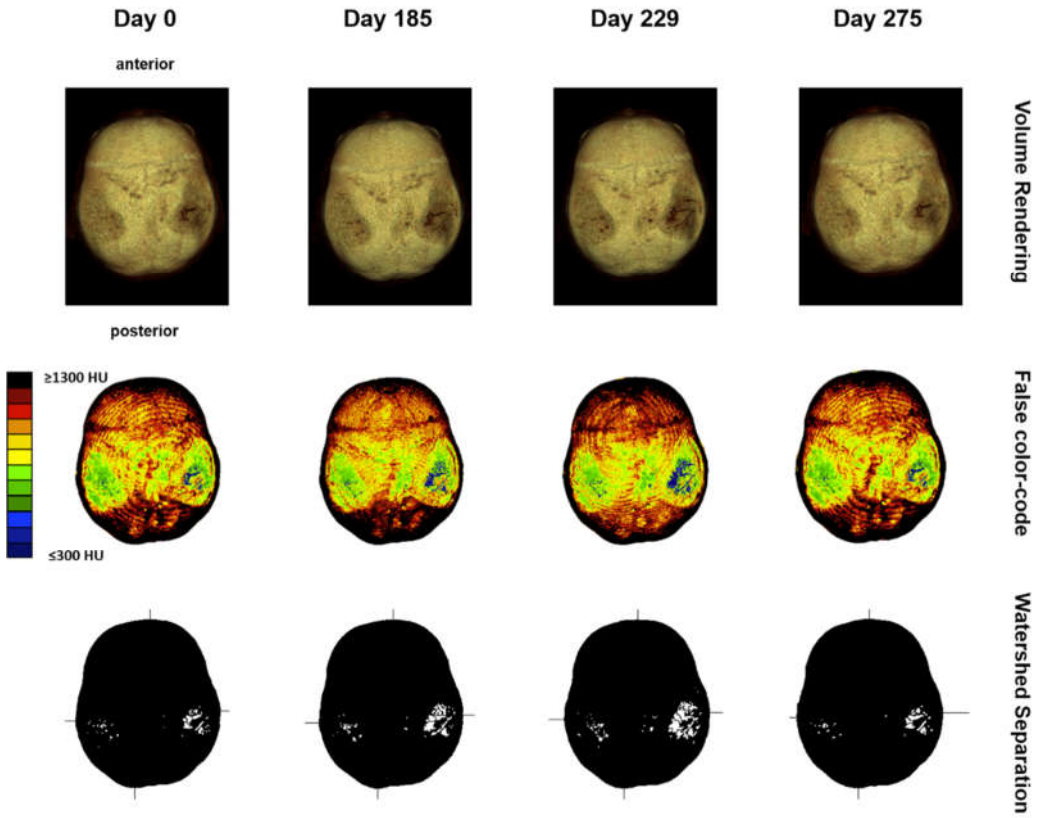

Figure 4. Maximum intensity projection with false color-code representation of 301 to 1300 HU of the skull bone showing progressive thinning on both parietal sides over time. Orientation is equalized for better comparison through registration using a 2D transformation with linear interpolation.

Preprints (www.preprints.org) | NOT PEER-REVIEWED | Posted: 23 April 2023 doi:10.20944/preprints202304.0749.v1

Next, volume rendering and maximum intensity projection of the skull were performed in all follow-up CTs, suggesting signs of disease progression, which justified further analyses to quantify the changes over time (Figure 4).

3.2. Two-dimensional (2D) measurements of biparietal thinning

The parietal bone was measured at the 3 thinnest points from days 0, 185, 229, and 275 (see Figure 5).

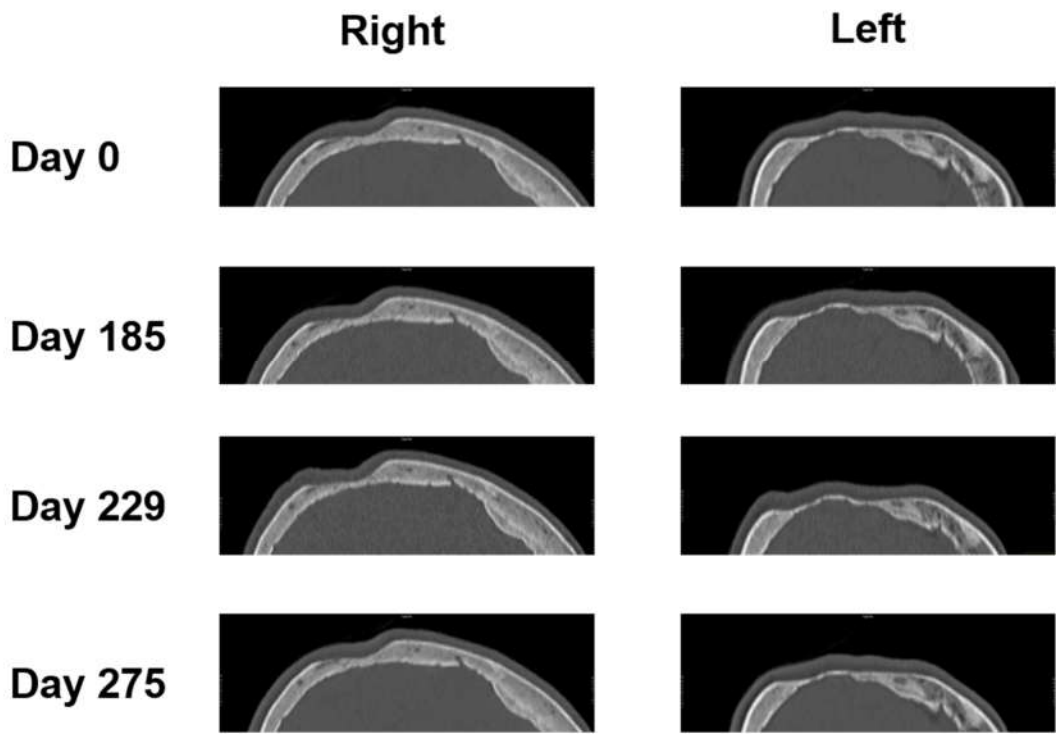

Figure 5. Sagittal CT images of a 75-year-old female patient from days 0 185, 229, and 275.

Then, 2D measurements were prepared in 3D head models for all 4 CT images with three points manually selected using the sample point tool (A, B, C for each side) and selection of the same points in the follow-up CTs (as depicted in Figure 1). Results of sample line measurements, sample point measurements, and particle analysis are shown in Figures 5 and 6, with deterioration of parietal thinning between day 0 and day 229 but without further deterioration between day 229 and 275, indicating stable disease without further bone loss despite treatment with corticosteroids. This finding parallels the improvement of headaches under treatment with corticosteroids. Only one value was available for particle analysis.

Preprints (www.preprints.org) | NOT PEER-REVIEWED | Posted: 23 April 2023 doi:10.20944/preprints202304.0749.v1

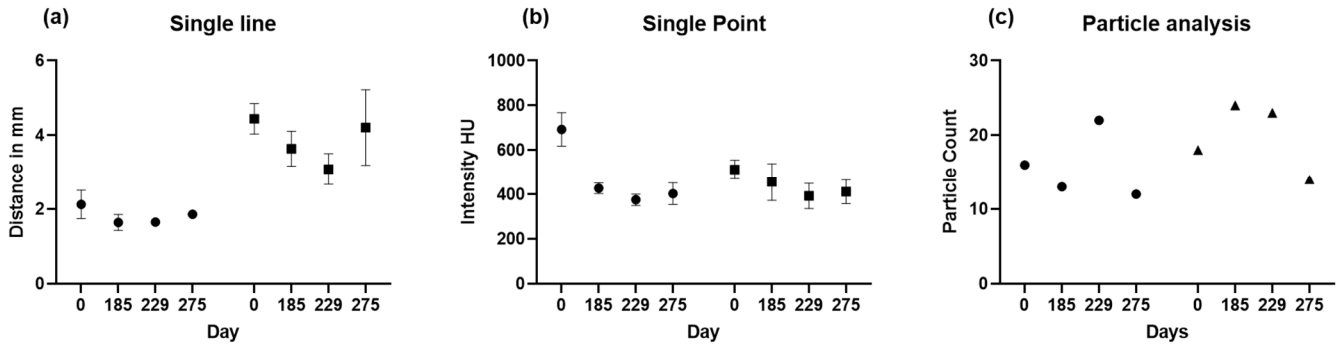

Figure 6. (**a**) Sample line (**b**) Sample point, and (**c**) particle analysis with 301 to 400 HU group summary plots are shown for the left and the right side. The means with standard deviations are displayed for the sample line and sample point.

3.3. Three-dimensional (3D) measurements of biparietal thinning

To further improve the quantification of bone loss over time, 3D measurements were planned using a CAD model. The preparation of the CAD model with an overlay on the Mesh format and skull alignment is shown in Figure 1. With average differences between the two models not exceeding 0.15 mm, the 3D reconstruction is considered reliable.

Using this 3D model, the parietal thicknesses can be displayed as a color map painted onto the surface (Figure 7). This method assures the complete mapping of bone thinning over the skull and clearly shows the two locations on the left and the right side.

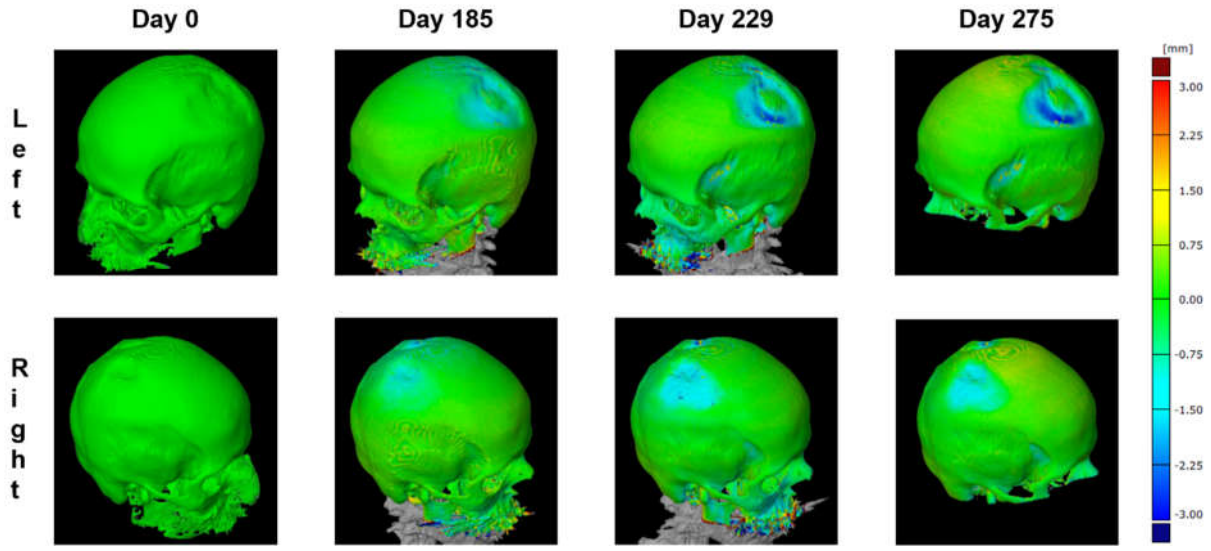

Figure 7. Two different perspectives of colored thickness mapping with defects up to -3mm between days 0 and 229 / 275.

Next, interfolding and volumetric measurements were calculated for both sides, as summarized in Figure 8. For volume analysis, no t-test is possible since there is only one value.

Preprints (www.preprints.org) | NOT PEER-REVIEWED | Posted: 23 April 2023 doi:10.20944/preprints202304.0749.v1

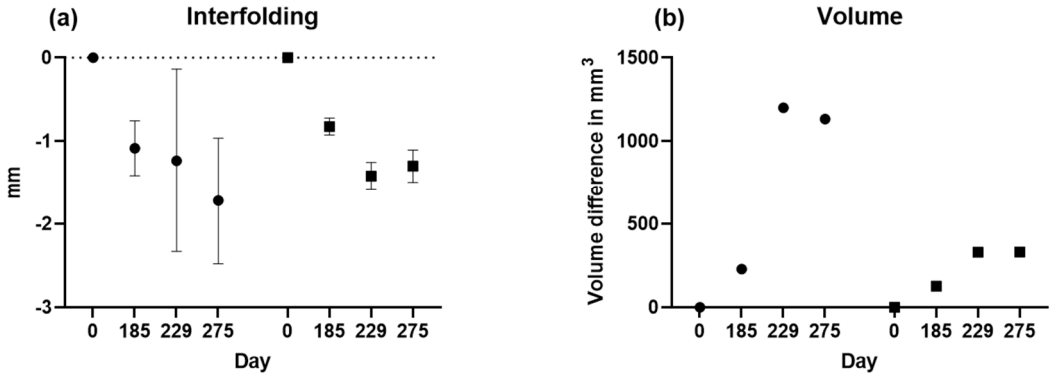

Figure 8. (**a**) interfolding and (**b**) volume group summary plots are shown for the left and the right side. Means with standard deviations are displayed for the interfolding.

3.4. Comparisons of changes in bone loss over time

A comparison of the results is presented in Figure 8 and Table 1. showing changes in bone loss over time when using different methods. Bone loss was significant between days 0 and 229, independent from the method applied, whereas bone loss was at least stable without significant deterioration between days 229 and 275.

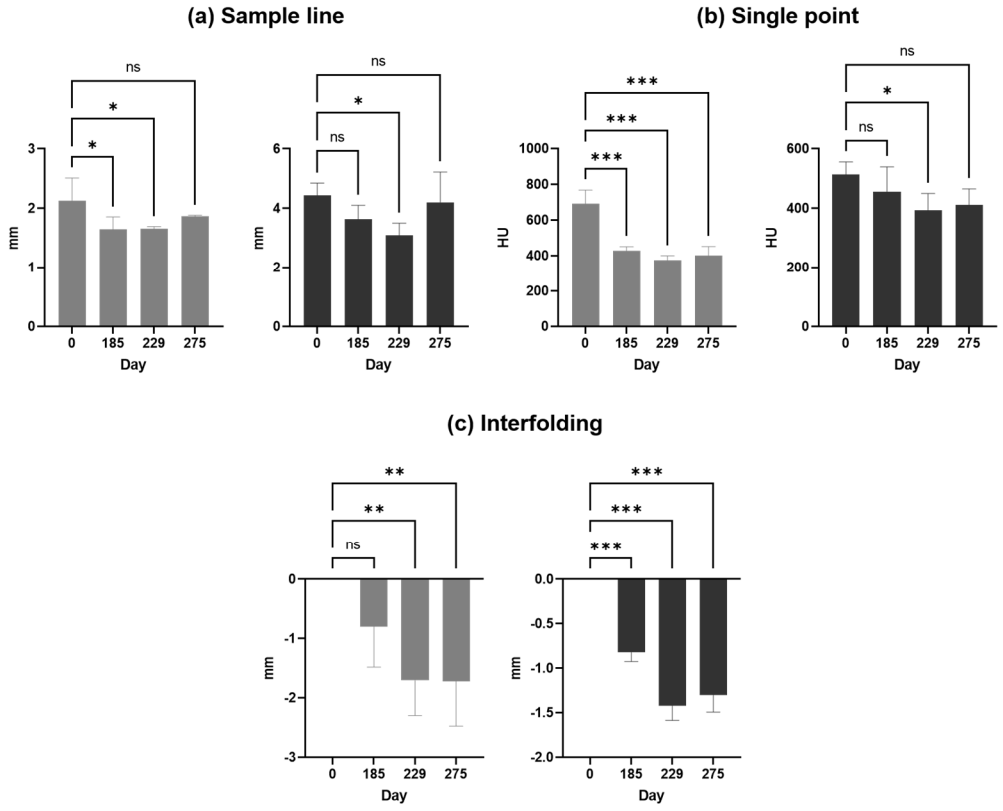

Figure 9. (**a**) Sample line, (**b**) single point, and (**c**) interfolding column bar graph are shown for the left (grey) and the right (black) side as means with standard deviations.

Preprints (www.preprints.org) | NOT PEER-REVIEWED | Posted: 23 April 2023 doi:10.20944/preprints202304.0749.v1

Table 1. Comparisons of bone loss were assessed by linear and volumetric measurements over time using the one-way ANOVA test and Fisher's LSD test for multiple comparisons.

			P-values based on one-way ANOVA			
Hemisphere	**Name**	**Units**	**0 vs. 185**	**0 vs. 229**	**0 vs. 275**	**229 vs. 275**
Right	Single Line	mm	0,1559^{ns}	0,0300*	0,6581^{ns}	0,0614^{ns}
	Single Point	HU	0,2840^{ns}	0,0420*	0,0755^{ns}	0,7166^{ns}
	Particle analysis	Counts	n.a.	n.a.	n.a.	n.a.
	Interfolding	mm	<0,0001***	<0,0001***	<0,0001***	0,3148^{ns}
	Volume	mm	n.a.	n.a.	n.a.	n.a.
Left	Single Line	mm	0,0263*	0,0287*	0,1747^{ns}	0,2745^{ns}
	Single Point	HU	0,0001***	<0,0001***	<0,0001***	0,4904^{ns}
	Particle analysis	Counts	n.a.	n.a.	n.a.	n.a.
	Interfolding	mm	0,1356^{ns}	0,0075***	0,0072***	0,9786^{ns}
	Volume	mm	n.a.	n.a.	n.a.	n.a.

*, significant, ***, highly significant difference between means; n.a., not assessable; ^{ns}, not significant

4. Discussion

This study summarizes the fundamental methodological approaches currently available to quantify bone loss in parietal thinning for follow-up comparisons. Despite using these methods only in CTs from a single patient, both 2D and 3D methods provided results that must be considered superior to a pure description of parietal thinning for comparative follow-up analyses. Most notably, the results show changes in parietal thinning, with significant deterioration and stable disease under clinical symptoms during follow-up.

All methods applied are based on CTs as an established, non-invasive medical imaging technique that produces detailed cross-sectional images of the body. Thus CT scans can provide both 2D-slices and 3D reconstructions of the human parietal bone, allowing multiple analyses of the parietal skull, with details focusing on structure and thickness. In 2D analyses, the thickness of the parietal bone is measured by taking a series of measurements along a single plane of the CT image. This method can provide accurate measurements of bone thickness, but it is limited in its ability to capture the complex 3D structure of the parietal bone. While 2D analysis is particularly useful for identifying local thinning or thickening of the bone, 3D analyses allow a more comprehensive view of the bone's structure, shape, size, and thickness. 3D analyses can further confirm the 2D data if available. Besides, 3D mapping appeared particularly useful for identifying patterns of thinning or thickening across the entire bone (Figure 7). The 3D reconstruction was reliable, with average differences between the two models not exceeding 0.15 mm. However, CT osteoabsorptiometry and densitogram patterns did not provide qualitative data for direct comparisons.

For this work, advanced imaging software tools have been used according to their availability in this institution, and a commercial partner specialized in CAD and Mesh modeling for industrial purposes. However, these methods are not approved for medical purposes and were applied only for this pivotal study. Nevertheless, the proposed techniques provided data for the treating physician and suggested a possible effect of corticosteroids in this individual patient. Although this workflow from 2D to 3D analyses could not be validated in a more extensive case series, it provides first

experiences which might be helpful even for interventional studies to monitor disease progression and evaluate the effectiveness of treatments.

Indeed, from the clinical perspective, the image analyses detailed above were considered helpful by the treating physicians. The stable disease under treatment with corticosteroids after day 229, correlating with a clear improvement of headaches, suggested a beneficial effect of corticosteroids concerning parietal bone loss and excluded further deterioration of bone loss as a possible side effect of corticosteroids. Only quantifying parietal bone loss allowed a comparison of the history of clinical symptoms like headaches with the potential consequences of corticosteroid treatment. To our knowledge, Lichen ruber has not been described to result in bone changes similar to Paget's bone disease. Although routine treatment of Lichen ruber does not include immunosuppressive agents like corticosteroids, histology has defined Lichen ruber with inflammatory reactions around the hair follicles, including diffuse lymhocytic infiltrates. According to the anatomical proximity, a cytokine-mediated effect of such an inflammatory process on the near skull could not be excluded.

Nevertheless, the complete pathophysiological mechanisms involved are still unclear, as bone biopsy was not considered because of possible complications close to the central nervous system. Bone metastasis, which occurs in about 10% of cases of gastric cancer [23], was excluded as a differential diagnosis based on the clinical course and ^{18}F-FDG-PET. Thus, the clinical management aim in this aged patient was to control the symptoms and stop or even improve parietal bone loss. Fortunately, corticosteroids resulted in stable disease with fewer headaches.

Due to the low prevalence of parietal thinning, even case series are rare for follow-up analyses and have not been reported in the literature. This report compares routine descriptive reports with quantitative analyses using 2D and 3D evaluations of bone defects. This patient's CTs showed increased bone loss independently from the methods applied between days 0 and 229. Indeed, a standard to quantify parietal bone loss cannot be derived from these data, and a multicentric study with more patients is necessary for directly comparing the proposed techniques. Any 2D and 3D evaluations provided helpful information for further treatment decisions.

Without a doubt, the main limitation of this work is the lack of more identified patients with follow-up CTs of this rare disease – both with and without therapeutic interventions. More data will allow further validation of the proposed analytical approaches, and it can be anticipated that 3D reconstructions and other image analyses will be helpful for diagnostic purposes and follow-ups. Specialized software approved for medical studies is needed for such investigations.

5. Conclusions

In conclusion, for routine radiological practice, at least 3D reconstruction of CTs with subsequent 2D analyses appears fully justified to increase the clinical awareness of the size of the parietal bone defects, allowing quantification of the bone loss during long-term follow-up. Additional 3D analyses may provide further information on patterns of bone thinning or thickening across the skull and allow the following changes in bone volumes over time. The description of parietal thinning alone is insufficient for follow-up imaging of parietal thinning.

Supplementary Materials: None

Author Contributions: Conceptualization, J.P. and M.S.; methodology, J.P. and A.P.; software,H.S.; formal analysis, J.P., A.P. and H.S.; writing—original draft preparation, J.P. and M.S.; writing—review and editing, all authors; visualization, J.P.; supervision, M.S.; funding acquisition, R.A. All authors have read and agreed to the published version of the manuscript.

Funding: This research received no external funding.

Institutional Review Board Statement: The study was part of a pilot study for structured documentation of patients' data (SolutionX) conducted in accordance with the Declaration of Helsinki, and approved by the Ethics Committee of the Medical University of Innsbruck (AN2017 -0041 370/4.18 453/AM2 (4581a)).

Informed Consent Statement: Informed consent was obtained from the patient involved in the study.

Data Availability Statement: The data presented in this study are available on request from the corresponding author. The data are not publicly available due to privacy reasons.

Acknowledgments: None.

Conflicts of Interest: The authors declare no conflict of interest. Authors must identify and declare any personal circumstances or interest that may be perceived as inappropriately influencing the representation or interpretation of reported research results. The funders had no role in the design of the study; in the collection, analyses, or interpretation of data; in the writing of the manuscript; or in the decision to publish the results.

References

1. Bruyn, G.W.; Bots, G.T.A.M. Biparietal osteodystrophy. *Clinical Neurology and Neurosurgery* **1978**, *80*, 125-148, doi:https://doi.org/10.1016/S0303-8467(78)80035-3.
2. Cvetković, D.; Bracanović, D.; Djonić, D.; Živković, V.; Djurić, M.; Nikolić, S. Biparietal osteodystrophy: Macroscopic appearance, computed tomography imaging and microarchitectural analysis. *Legal Medicine* **2022**, *55*, 102025, doi:https://doi.org/10.1016/j.legalmed.2022.102025.
3. Cederlund, C.G.; Andrén, L.; Olivecrona, H. Progressive bilateral thinning of the parietal bones. *Skeletal Radiology* **1982**, *8*, 29-33, doi:10.1007/BF00361365.
4. Camp, J.D.; Nash, L.A. Developmental Thinness of the Parietal Bones. *Radiology* **1944**, *42*, 42-47, doi:10.1148/42.1.42.
5. Barnes, E. *Developmental defects of the axial skeleton in paleopathology*; University Press of Colorado: 1994.
6. Poor, G.; Donath, J.; Fornet, B.; Cooper, C. Epidemiology of Paget's disease in Europe: the prevalence is decreasing. *J Bone Miner Res* **2006**, *21*, 1545-1549, doi:10.1359/jbmr.060704.
7. von Rokitansky, C. *Handbuch der allgemeinen pathologischen Anatomie*; Braumüller & Seidel: 1842.
8. Greig, D.M. On symmetrical thinness of the parietal bones. *Edinburgh Medical Journal* **1926**, *33*, 645.
9. Grainger, R.G.; Allison, D.J. *Grainger & Allison's diagnostic radiology: a textbook of medical imaging*; Churchill Livingstone: 1997; Volume 1.
10. Nashold, B.S., Jr.; Netsky, M.G. Foramina, Fenestrae, and Thinness of Parietal Bone*. *Journal of Neuropathology & Experimental Neurology* **1959**, *18*, 432-441, doi:10.1097/00005072-195907000-00005.
11. De Stefano, G.F.; Hauser, G.; Guidotti, A.; Rossi, S.; Russo, E.G.; Gualandi, P.B. Reflections on interobserver differences in scoring non-metric cranial traits (with practical examples). *Journal of Human Evolution* **1984**, *13*, 349-355, doi:https://doi.org/10.1016/S0047-2484(84)80041-X.
12. Tsutsumi, S.; Yasumoto, Y.; Ito, M. Idiopathic calvarial thinning. *Neurol Med Chir (Tokyo)* **2008**, *48*, 275-278, doi:10.2176/nmc.48.275.
13. Deshpande, N.; Hadi, M.S.; Lillard, J.C.; Passias, P.G.; Linzey, J.R.; Saadeh, Y.S.; LaBagnara, M.; Park, P. Alternatives to DEXA for the assessment of bone density: a systematic review of the literature and future recommendations. *Journal of neurosurgery. Spine* **2023**, 1-10, doi:10.3171/2022.11.Spine22875.
14. Martel, D.; Monga, A.; Chang, G. Osteoporosis Imaging. *Radiologic Clinics of North America* **2022**, *60*, 537-545, doi:https://doi.org/10.1016/j.rcl.2022.02.003.
15. Pfeil, A.; Lehmann, G.; Lange, U. Update DVO-Leitlinie 2017 „Prophylaxe, Diagnostik und Therapie der Osteoporose bei postmenopausalen Frauen und Männern". *Zeitschrift für Rheumatologie* **2018**, *77*, 759-763, doi:10.1007/s00393-018-0549-8.
16. Poilliot, A.; Doyle, T.; Kurosawa, D.; Toranelli, M.; Zhang, M.; Zwirner, J.; Müller-Gerbl, M.; Hammer, N. Computed tomography osteoabsorptiometry-based investigation on subchondral bone plate alterations in sacroiliac joint dysfunction. *Scientific reports* **2021**, *11*, 8652, doi:10.1038/s41598-021-88049-2.
17. Müller-Gerbl, M. The subchondral bone plate. *Advances in anatomy, embryology, and cell biology* **1998**, *141*, Iii-xi, 1-134, doi:10.1007/978-3-642-72019-2.

18. Hoechel, S.; Wirz, D.; Müller-Gerbl, M. Density and strength distribution in the human subchondral bone plate of the patella. *International orthopaedics* **2012**, *36*, 1827-1834, doi:10.1007/s00264-012-1545-2.
19. Serrano, N.; Kissling, M.; Krafft, H.; Link, K.; Ullrich, O.; Buck, F.M.; Mathews, S.; Serowy, S.; Gascho, D.; Grüninger, P.; et al. CT-based and morphological comparison of glenoid inclination and version angles and mineralisation distribution in human body donors. *BMC Musculoskeletal Disorders* **2021**, *22*, 849, doi:10.1186/s12891-021-04660-4.
20. Gay, M.H.; Born, G.; Mehrkens, A.; Wittig, H.; Müller-Gerbl, M. Computed tomography osteoabsorptiometry for imaging of degenerative disc disease. *North American Spine Society journal* **2022**, *9*, 100102, doi:10.1016/j.xnsj.2022.100102.
21. Schindelin, J.; Arganda-Carreras, I.; Frise, E.; Kaynig, V.; Longair, M.; Pietzsch, T.; Preibisch, S.; Rueden, C.; Saalfeld, S.; Schmid, B.; et al. Fiji: an open-source platform for biological-image analysis. *Nature Methods* **2012**, *9*, 676-682, doi:10.1038/nmeth.2019.
22. Stefaniak, J.; Kubicka, A.M.; Wawrzyniak, A.; Romanowski, L.; Lubiatowski, P. Reliability of humeral head measurements performed using two- and three-dimensional computed tomography in patients with shoulder instability. *International orthopaedics* **2020**, *44*, 2049-2056, doi:10.1007/s00264-020-04710-x.
23. Aiba, H.; Nakazato, T.; Matsuo, H.; Kimura, H.; Saito, S.; Sakai, T.; Murakami, H.; Kawai, J.; Kawasaki, S.; Imamura, Y. Bone Metastases from Gastric Cancer Resembling Paget's Disease: A Case Report. *J Clin Med* **2022**, *11*, doi:10.3390/jcm11247306.